Pharmacological Research 226 (2026) 108145

Contents lists available at ScienceDirect

Pharmacological Research

journal homepage: www.elsevier.com/locate/yphrs

TSPO-mediated mitochondrial retrograde signaling primes the microglial NLRP3 inflammasome

Aarti Singh [a,1], Manuel Rigon [b,1], Tong Guo [b,1], Danilo Faccenda [b,e], Gopinath Lakshmanan [b], Dong Xia [a], Marta Gramaça Caldeira [a], Jordi Lopez-Tremoleda [d,e], Zahra Falah Hassan Al-Khateeb [d,e], Rosella Abeti [c], Paola Giunti [c], Michelangelo Campanella [b,f,g,*]

[a] Department of Comparative Biomedical Sciences, The Royal Veterinary College, University of London, London NW1 0TU, United Kingdom
[b] William Harvey Research Institute, Queen Mary University of London, EC1M 6BQ London, United Kingdom
[c] Ataxia Centre, Department of Clinical and Movement Neurosciences, UCL Queen Square Institute of Neurology, Queen Square, London WC1N 3BG, United Kingdom
[d] Barts Centre for Trauma Sciences, Blizard Institute, Queen Mary University of London, E1 2AT London, United Kingdom
[e] Department of Clinical, Pharmaceutical and Biological Science, University of Hertfordshire, Hatfield AL10 9AB, United Kingdom
[f] CNRS UMR9018, Université Paris-Saclay, Gustave Roussy, Villejuif, France
[g] Department of Biomedical Sciences, University of Padua, 35131, Italy

ARTICLE INFO

Keywords:
Mitochondria
Neuroinflammation
Mitophagy
NLRP3 and TSPO

ABSTRACT

Uncontrolled microglial activation is a central driver of neuroinflammatory brain diseases. The mitochondrial translocator protein (TSPO) is a well-established molecular signature of brain inflammation and serves as a diagnostic marker. However, despite this strong association, it remains unclear whether TSPO acts as a positive or negative regulator of microglial function and how it influences the inflammatory and healing responses that follow brain injury. Moreover, recent evidence of species-specific differences in TSPO expression underscores the need to better define its biology in brain-resident macrophages. Here, using a murine microglial model, we demonstrate that TSPO is required for the mitochondrial priming of inflammation and acts as a conduit for its amplification. This function relies on the engagement of multiple intracellular pathways and can be effectively counteracted by the tricyclic indole compound GE-180. Specifically, in response to inflammatory stimuli, TSPO (i) stabilizes on the mitochondrial membrane where it binds and sequesters NOD-like receptor (NLR) proteins, (ii) represses PARK2-mediated mitophagy, and (iii) promotes nuclear retrograde signaling through NF-κB accumulation, thereby enhancing the expression of pro-inflammatory genes. Sustained TSPO-dependent inflammation further drives cellular demise and excitotoxicity. Collectively, these findings advance our understanding of TSPO's molecular physiology in microglia, highlight its pivotal role in mitochondrial control of inflammation, and identify TSPO as a promising target for the pharmacological modulation of neuroinflammatory responses.

1. Introduction

Microglia are the CNS resident immune cells which respond rapidly to external stimuli by switching from a "resting state" to a surveillance mode, to various states of activation [1]. This evolution is accompanied by a radical cellular morphological change and release of a specific subset of cytokines that vary from pro-inflammatory (e.g. IL-1β, IL-6, IL-12, TNFα, CD86 and iNOS) [2,3]to anti-inflammatory (e.g. IL-4, IL-10, IL-13, TGF-β and CD206) [4].

A prerequisite for microglial activation is the intracellular accumulation and assembly of the nucleotide oligomerization domain (NOD)-like receptor family pyrin domain-containing 3 (NLRP3) inflammasome. The inflammasome is a complex composed of NLRP3 (i), the adaptor molecule apoptosis-associated speck-like protein containing a caspase recruitment domain (ASC) (ii) and caspase 1 (CASP-1) (iii). The abnormally increased formation of this complex is implicated in the

* Corresponding author at: William Harvey Research Institute, Queen Mary University of London, EC1M 6BQ London, United Kingdom.
E-mail address: m.campanella@qmul.ac.uk (M. Campanella).
[1] Equally contributed

https://doi.org/10.1016/j.phrs.2026.108145
Received 3 November 2025; Received in revised form 16 February 2026; Accepted 16 February 2026
Available online 19 February 2026

pathogenesis of several chronic pathologies (e.g. Alzheimer's disease [AD], Parkinson's disease [PD], multiple sclerosis [MS] and amyotrophic lateral sclerosis [ALS]).

Upon its assembly, the inflammasome triggers the autocleavage of the Caspase-1 protein, activating it. Once cleaved and active, CASP-1 can then process the proinflammatory cytokines pro-IL-1β and pro-IL-18 into their biologically active mature forms [5], thereby enhancing inflammation and leading to an inflammatory pyroptotic cell death.

Studies have demonstrated that mitochondria are crucial for NLRP3 inflammasome activation [5,6]. Mitochondrial damage induced by NLRP3 activators mediates the externalization of mitochondria-derived molecules, including cardiolipin and mtDNA.

This event allows the mitochondrial recruitment and assembly of NLRP3, leading to inflammasome activation [7,8]. Consequently, the autophagic removal of damaged mitochondria reduces NLRP3-mediated inflammatory response [9].

The translocator protein (TSPO) is an evolutionarily conserved five-transmembrane domain protein that localizes to the outer mitochondrial membrane (OMM) [10]. While TSPO is ubiquitously expressed in mammalian systems, the protein is found at high levels in tissues with active lipid metabolism [11]. TSPO is primarily involved in regulating mitochondrial cholesterol influx and steroidogenesis[12]. More recently, biochemical and pharmacological studies have unveiled that TSPO takes part in a plethora of cell pathways encompassing mitophagy (i), Ca^{2+} signalling (ii) and reactive oxygen species (ROS) generation (iii).

The protein level of TSPO is upregulated in several disease-associated conditions including cancer and central nervous system (CNS) inflammation [13,14]. TSPO-binding drugs are enrolled on a vast spectrum of therapeutic interventions ranging from anti-neuroinflammatory treatments [15,16] to chemotherapy [17–19] and anxiolysis [3]. TSPO-ligands, such as the isoquinoline PK11195 have been applied for the diagnostic imaging of brain injury, during which increased TSPO expression is associated with neuroinflammatory damage. Targeting of TSPO is therefore used to measure brain inflammation both in experimental models and human patients [20,21].

Recent findings suggest that reduced autophagic competence promotes pro-inflammatory microglial polarisation [22]. Taken together, the above evidence raised the speculation that TSPO is involved in inflammasome signalling pathways as TSPO is indicated to counteract mitochondrial autophagy. Alternatively, early work suggested that TSPO modulates mitochondrial retrograde signaling, between mitochondira and the nucleus, thereby changing the dynamics of transcription factors, such as the NF-κB which is key to he inflammatory signalling cascade [23,24].

However, the molecular details, especially the interplay between TSPO, mitochondria and NLRP3 inflammasome activation, are still elusive. Therefore, it remains difficult to elaborate on the role of TSPO during microglial activation.

In the current study, we demonstrate that TSPO mediates inflammasome signalling in microglia cells. Along with the repression of mitophagy, TSPO sustains the scaling of the inflammatory response in microglial cells via the stabilization of the NLRP3 on the mitochondria and exploitation of the retrograde signalling. A complex scaling of inflammation which irreversibly drives microglial cells to death.

2. Material and methods

2.1. Cell culture and transfection

BV2 microglial cells (ATCC) were maintained in a temperature-controlled, humidified incubator at 37 ℃ with 5 % CO_2 (Hera Cell 240, Thermo Scientific, Essex, UK). TSPO KO microglia were generated using GeneArt™ CRISPR Nuclease Kit (Invitrogen, A21174) and maintained like the Wild Type (WT) BV2. The cells were cultured in Dulbecco's Modified Eagle Medium (DMEM) containing High Glucose (25 mM), L-Glutamine (4 mM) and Sodium Pyruvate (1 mM) (Thermo Fisher, 11995065), supplemented with 10 % Fetal Bovine Serum (FBS) (Thermo Fisher, 10082147) and 1 % of 100 U/mL Penicillin and 100 mg/mL streptomycin (Thermo Fisher, 15140122). GE-180 was a gist by General Electric Healthcare. Transfection was performed using Lipofectamine 3000 transfection reagent (Thermo Fisher, L3000015) according to the manufacturer's instructions and following optimization.

2.2. Immunocytochemistry (ICC)

Cells were seeded onto Nunc™ Lab-Tek™ II Chamber Slide™ System (Thermo Fisher, 154534PK) treated and/or transfected as described. After treatment, cells were washed twice using 0.01 M Phosphate Buffered Saline (PBS 1X) and fixed using 4 % paraformaldehyde (PFA) solution for 15 min at RT. After 3X washes with PBS permeabilization was made with 0.3 % Tritonx-100 for 15 min. The cells were subsequently washed with PBS (3X) for 10 min incubation periods. The slides were blocked for 1 h in 5 % FBS (blocking buffer) at RT and incubated overnight at 4°C in a humidified chamber after the addition of primary antibody diluted in blocking buffer. The slides were then washed 3x15mins using PBS-T (PBS with 0.2 % Tween) and then incubated with secondary antibody in PBS-T for 1–2 h at RT. The secondary antibodies were conjugated to Alexa Fluor dyes (Life Technologies, UK). Following washing (3 ×15 min using PBS-T) in the dark slides were mounted using 4', 6-diamidino-2-phenylindole (DAPI) mounting solution (Abcam, ab104139).

2.3. Immunohistochemistry (IHC)

For the IHC, a total of 8 adult, 10-week-old male mice, weighing 30–34 g (Charles River Laboratories, Margate, UK), were used. Mice were housed in an Individually Ventilated Cage (IVC; Allentown Europe, UK), in a 12 h light-dark cycle, with controlled room temperature (21 ± 1°C) and relative humidity (40–60 %) and with diet and water ad libitum. All animal procedures were carried out under a Project Licence approved by the Animal Welfare and Ethical Review Body, at Queen Mary University of London and the UK Home Office, by the EU Directive 2010/63/EU. Animals were subjected to controlled cortical impact (CCI) injury. Briefly, animals were acclimatised for 1-week after arrival to the animal unit. Mice were anaesthetised (ketamine 50 mg/kg and medetomidine 0.5 mg/kg; IP) and placed in a stereotaxic frame. A right lateral craniotomy was carried out, 2.0 mm behind bregma and 2.5 mm lateral to the midline and a CCI injury was induced using a 3 mm impactor tip with a speed of 3 m/s, a depth of 2.2 mm and a dwell time of 100 ms, applied with the PCI3000 Precision Cortical Impactor™ (Hatteras Instruments, Inc., US). After the injury, the skull flap was placed back unfixed to allow for expansion, and the skin was sutured. Buprenorphine (0.05 mg/kg, s.c.) was used in all animals pre-operatively for pre-emptive analgesia and post-operatively every 12 h for 3 days post-surgery. Naïve animals were used as controls. Slides were scanned at x40 using the In Cell Analyser 2200 (INCA2200) System (Cytiva, Marlborough, United States) and the In Cell Developer Toolbox v1.9.2 (Cytiva, Marlborough, United States) was used to quantify the signal. Image processing was done using ImageJ software (National Institutes of Health, Bethesda, USA).

2.4. Proximity ligation assay (PLA)

PLA assay was performed according to manufacturer's instructions. Cells were seeded in 8-well chamber slides and fixed in 4 % PFA in PBS after 24 h. PLA was performed by using the Duolink® PLA Red reagents (Sigma-Aldrich, DUO92008). Cells were permeabilised with 0.2 % Triton X-100 in PBS for 10 min at RT. Blocking was performed with the Duolink® Blocking Solution for 1 h at 37 °C. Cells were incubated with a primary antibody solution containing anti-NLRP3 (Adipogen, AG-20B-0014-C100) and anti-SDHA (Cell Signaling Technology, 5839S)

prepared in Duolink® Antibody Diluent overnight at 4°C in a humidified chamber. After primary antibody incubation, cells were washed twice in 1x Wash Buffer A for 5 min at RT and then incubated with PLA probe solution containing Duolink® In Situ PLA® Probe Anti-Rabbit PLUS and Probe Anti-Mouse PLUS for 1 h at 37 °C, followed by two washes with 1x Wash Buffer A for 5 min. Ligation was performed for 30 min at 37 °C After two washes with 1x Wash Buffer A for 5 min, amplification was performed in a humidity chamber for 100 min at 37 °C in dark. Amplification was followed by two washes with 1x Wash Buffer B for 10 min, and then one wash with 0.01x Wash Buffer B for 1 min. A cover glass was then mounted using a mounting medium with DAPI (Abcam, ab104139). Three negative control samples (anti-NLRP3 only, anti-SDHA only and no antibody, respectively) were also included to verify the specificity of the PLA signal.

2.5. RT-qPCR

RNeasy Plus mini kit (Qiagen, 74134) was employed to extract the RNA according to the manufacturer's instructions and then quantified using NanoDrop spectrophotometer (ThermoFisher Scientific). Quantinova Reverse Transcription Kit (Qiagen, 205413) was used according to the manufacturer's instructions to transcribe the RNA to cDNA. The 2X Quantinova SYBR green master mix (Qiagen, 204141). The qPCR reaction was performed in 384 well plates in triplicate reactions. The mean Ct was normalized to the Ct for a housekeeping gene (GAPDH). The delta Ct (ΔCt) was calculated: gene of interest Ct – housekeeping gene Ct. From this, the relative mRNA content is calculated using the following formulae: $2^{\hat{}-\Delta\Delta}$Ct. The mean $2^{\hat{}-\Delta\Delta}$Ct was calculated from the 4–5 independent experiments. Sequences of Primers are reported in Table 1.

2.6. Immunoblotting

Protein concentrations were quantified using the Detergent compatible (DC) protein assay (Bio Rad, 5000112) according to manufacturer instructions. The absorbance was subsequently read using a plate reader (Tecan Infinite M200 Pro, UK) at 695–750 nm with a BSA standard curve used to determine the protein concentration (μg/μL) of the samples. The volume of protein required to achieve 20 μg of sample was loaded onto 12 % polyacrylamide gels. Bio-Rad Mini-PROTEAN tetra system electrophoresis unit was used. After transfer the blots were blocked in 5 %(w/v) solution of milk powder in TBS-T (50 mM Tris, 150 mM NaCl, 0.05 % Tween 20 (Sigma, P9416)) for 1 h at RT. The membrane was incubated with antibodies diluted in milk at 4°C overnight. Following primary antibody incubation, the membranes were washed 3x5min with 5 % (w/v) solution of milk powder in TBS-T at RT. The membrane was incubated for 2 h with the corresponding peroxidase-conjugated secondary antibody diluted in milk. Membranes were washed (3x5min) in TBS-T. To visualize the blot, the ECL western blotting detection kit (Amersham, RPN2133) was utilized. Imaging and visualization were performed using a ChemiDoc™ MP System (Bio-Rad, 1708280).

Table 1
Caption.

Gene	Forward Primer	Reverse Primer
Tspo	ACTGTATTCAGCCATGGGGTA	ACCATAGCGTCCTCTGTGAAA
IL-6	GATGGATGCTACCAAACTGGAT	CCAGGTAGCTATGGTACTCCAGA
iNos	CTTTGCCACGGACGAGAC	TCATTGTACTCTGAGGGCTGA
Nlrp3	TGCTCTTCACTGCTATCAAGCCCT	ACAAGCCTTTGCTCCAGACCCTAT
Gapdh	CCATGGAGAAGGCTGGGG	CAAAGTTGTCATGGATGACC
Atp5β	GGCACAATGCAGGAAAGG	TCAGCAGGCACATAGATAGCC
TNF-a	AAATGGGCTCCCTCTCATCAGTTC	TCTGCTTGGTGGTTTGCTACGAC
IL-1β	CACCTCTCAAGCAGAGCACAG	GGGTTCCATGGTGAAGTCAAC
Caspase 1	CCCAGAAGTTATGGAAAGAAAATCCTTCAG	GGATACCATGAGACATGAATACAAGGAAAG
ASC	CAGAGTACAGCCAGAACAGGACAC	GTGGTCTCTGCACGAACTGCCTG
IL-10	ATAACTGCACCCACTTCCCA	GGGCATCACTTCTACCAGGT

2.7. Co-Immunoprecipitation

Microglia BV2 WT cells and BV2 TSPO KO cells were seeded in 6-well plates and treated with LPS 100 ng/mL for 24 h or LPS 100 ng/mL for 24 h + 2.5 mM ATP for 30 min. After treatment, the cells were washed twice in PBS and subsequently lysed with standard Lysis buffer (150 mM NaCl, 1 % Triton in 50 mM Tris-HCL, pH 8) and protein concentrations were determined via DC protein assay as described above. For the immunoprecipitation assay, 1 ug of TSPO antibody (abcam, ab108489) has been added to 50 μl of magnetic beads linked to Protein A (ThermoFisher Scientific, 10001D) for 15 min at RT to induce the binding. After the incubation, the beads were washed twice with PBS and incubated overnight with 100 ug of total protein from the samples obtained above. The next day, the Flow Through (FT) fraction was collected, and the beads were washed twice with PBS. Finally, the proteins attached to the beads and the TSPO antibody have been eluted by adding 60 μL of Loading Buffer (375 mM Trsi-HCL pH 6.8, 6 % SDS, 4.8 % Glycerol, 9 % β-mercaptoethanol, 0.03 % bromophenol blue) and boiling the samples for 10 min, obtaining this way the IP fraction for the Western Blot analysis.

2.8. Cholesterol assay

The Amplex Red Cholesterol Assay Kit (Thermo Fisher, A12216 was used to quantify cholesterol levels. Cells were resuspended in the 1X reaction buffer (0.1 M potassium phosphate, pH 7.4, 0.05 M NaCl, 5 mM cholic acid, 0.1 % Triton X-100) that was supplied with the kit. The suspension was aliquoted in triplicate in 96-well plates. Amplex Red reagent containing 2 U/mL HRP, 2 U/mL cholesterol oxidase, and 0.2 U/mL cholesterol esterase was prepared according to the kit instructions. The reaction was incubated at 37 °C for 30 min (in the dark). The subsequent change in fluorescence was measured in a Tecan M200 Pro Plate Fluorescence microplate reader (Tecan, UK) using excitation at 544 nm and emission at 590 nm.

2.9. Reactive oxygen species (ROS) analysis

Dihydroethidium (DHE) is sensitive to O^{2-} and oxidises to 2-hydroxyethidium and the rate at which the nuclear signal rises in intensity correlates with cytosolic levels of superoxide. Cells were seeded on 22 mm glass coverslips and treated for 24 h with Vehicle or LPS. 24 h post-treatment cells were washed using room temperature PBS 1X and transferred to Attofluor Cell Chamber (Sigma Aldrich, A7816), 5 μM of DHE was added in HBBS medium (Hanks' Balanced Salt Solution, Thermo Fisher, 24020117), and the increase in intensity measured continuously over time using a UV Nikon microscope.

2.10. Nitric oxide (NO2) levels analysis

The Griess reaction allows for the spectrophotometric detection of nitrite formed by the oxidation of NO, quantified using a microplate reader at an absorbance of 548 nm. Cells were seeded and treated in triplicate on 96-well plates 48 h prior to the experiment. Sample media was used alongside photometric references made using the Griess reagent diluted in deionised water and sodium nitrite standards (1 – 100 μM) and quantified according to the manufacturer's instructions.

2.11. Cytotoxicity assessment

LDH (lactate dehydrogenase) activity assay (Merck) is a colorimetric assay used to measure the concentration of LDH in the cell culture medium. Microglial BV2 cells were seeded in 25 cm^2 flasks and either cultured for 48 h or cultured for 24 h and then treated using LPS for another 24 h. The microglial conditioned medium was collected, filtered, and used to treat neuroblastoma N2a cells for 24 h. N2a cells were also treated with complete medium and complete medium supplemented with 5 μM glutamate. N2a cells seeded in triplicate in the same plate and treated with complete medium only were used as a negative control, whereas N2a cells seeded in triplicate in the same plate and treated with glutamate were used as a positive cytotoxicity control. The average absorbance values of the triplicate samples were calculated. Cytotoxicity % for each of the conditions was calculated using the formula recommended by the kit company: (experimental value -negative control)/(positive control - negative control) *100. Cytotoxicity % was further normalised to be expressed as a percentage to the WT + Vehicle condition. The experiment was repeated 6 times, with BV2 and N2a cells being seeded on 6 different days. LDH activity was assessed following the manufacturer's instructions. Sample absorbance was read at 409/492 nm with a Tecan Sunrise plate reader.

2.12. Transcriptome data analysis

Total RNA samples were extracted using Quick-RNA Miniprep (Zymo Research, USA) according to the manufacturer's instructions and then quantified with an Agilent 2100 bioanalyzer. The quantified RNA samples were used for NEBNext® rRNA-depleted (Human/Mouse/Rat) stranded library preparation. Library preparation and RNA sequencing were conducted at the UCL Genomics. Libraries were prepared using non-strand specific Illumina TruSeq Sample Preparation Kits followed by Illumina sequencing. FASTQ files were aligned using TopHat and Cufflinks. Normalization and differential analyses were carried out using R software Bioconductor[61] package DESeq2 [62], and gene set enrichment analysis (GSEA) was carried out using EGSEA [63]. For gene expression profiling, the lists of genes belong to NLRP3 inflammasome complex and autophagosome were retrieved with Gene Ontology accession GO:0072559 and GO:0005776 respectively. Genes involved in mitophagy were retrieved from GO:0000423 and Reactome accession R-HSA-5205647.

Methods for the assessment of Ca^{2+} signalling, Oxygen Consumption Rate (OCR), mitochondrial membrane potential ($\Delta\Psi_m$), cellular viability, and GE-180 binding are reported in the Supplementary Material**.**

2.13. Statistical analysis

Three biological and technical replicates have been attained for each of the experiments. All statistical analyses were performed in GraphPad Prism 9.0 (GraphPad software, USA). Data are presented as mean ± standard error of the mean (SEM). Variations between three or more independent groups were determined using one-way analysis of variance (ANOVA). Two-way ANOVA with randomized block was used to evaluate differences between groups while accounting for the day block effect. Tukey's post hoc test was used to reveal all possible pairs of means within the data sets. P values of less than 0.05 was considered significant ($P < 0.05$ *; $P < 0.01$ **; $P < 0.001$ ***; $P < 0.0001$ ****).

3. Results

3.1. TSPO regulates the pro-inflammatory activation capacity of immune cells

Our previous data further demonstrated that treatment of BV2 microglial cells with lipopolysaccharides (LPS) significantly increased TSPO protein levels, suggesting a close link between TSPO expression and pro-inflammatory (M1) polarization of microglia under infection conditions [25]. In our current study, we additionally found that when BV2 cells were treated with anti-inflammatory cytokine interleukin-4 (IL-4) [26], TSPO expression was significantly reduced compared to untreated cells (**Figure 1ac**, **bd**). Together, these findings demonstrate a robust correlation between TSPO expression and microglial activation. The immunohistochemistry (IHC) results showed that in mice with traumatic brain injury, TSPO was markedly enriched in Iba1-positive microglial cells (Supplementary Figure 1a**, b**). To further elucidate the role of TSPO in microglial activation, we generated a TSPO-knockout (KO) BV2 cell line using CRISPR/Cas9 technology (Supplementary Figure 1c**-f**). The knockout efficiency was confirmed by western blotting and by assessing intracellular cholesterol distribution (Supplementary Figure 1 **g**), given that TSPO functions as an established intracellular cholesterol transporter [27]. KO cells exhibited higher mitochondrial metabolic activity than wild-type (WT) cells under basal conditions (Fig. 1**c-f**). Upon LPS stimulation, the mitochondrial oxygen consumption rate (OCR) decreased in both WT and KO cells. However, KO cells maintained significantly higher OCR levels compared to untreated WT cells. In parallel, DHE staining revealed that LPS-treated WT cells exhibited higher cytosolic ROS levels compared with KO cells (Fig. 1**g**).

Consequently, we measured the expression levels of key pro-inflammatory markers, including the mRNA levels of interleukin-1β and iNOS, as well as the protein level of NLRP3 (Fig. 1**h-k, Supp. Figure 1j-m**). In WT cells, all three markers were significantly upregulated following LPS treatment, indicating effective priming of the inflammasome pathway. In contrast, such induction was abolished in TSPO-deficient cells. Finally, immunocytochemistry (ICC) analysis showed colocalization between TSPO and NLR family pyrin domain containing 3 (NLRP3) (Fig. 1**n**).

3.2. TSPO modulates pro-inflammatory signalling by regulating inflammasome assembly

Based on the results described above, we next investigated how TSPO regulates the behaviour of NLRP3 during inflammation activation.

It has been widely reported that BV2 cells can be stimulated into a reactive, inflammatory phenotype by multiple stimulators, including lipopolysaccharide (LPS) [28–30].To track the subcellular dynamics of NLRP3 throughout the priming and activation stages, BV2 cells were first treated with LPS for 24 h (priming) and subsequently exposed to ATP for 30 min (activation). Immunocytochemistry (ICC) analysis revealed that in WT BV2 cells, LPS treatment not only induced an upregulation of NLRP3 but also promoted its recruitment to mitochondria (Fig. 2**a**), as evidenced by a significant increase in the colocalization coefficient between NLRP3 and ATPB (Fig. 2**b**). ATP stimulation further triggered the clustering of NLRP3, consistent with inflammasome formation. In contrast, in TSPO-KO BV2 cells, the expression level of NLRP3 remained unchanged after both LPS and LPS + ATP treatments. Moreover, the LPS-induced mitochondrial recruitment of NLRP3 observed in WT cells was abolished in the absence of TSPO. These results indicate that TSPO is required for the mitochondrial localisation of NLRP3 during inflammatory activation. Supporting the ICC findings, co-immunoprecipitation analysis in WT BV2 cells revealed a dynamic interaction between NLRP3 and TSPO: a minor basal interaction was detected under resting conditions, which markedly increased upon LPS stimulation. When the LPS-primed cells were subsequently triggered by ATP, NLRP3 dissociated from TSPO, consistent with its release for inflammasome assembly (Fig. 2**c, d**). Unlike NLRP3, the mitochondrial localisation and aggregation of ASC were not affected by TSPO knockout (**Supp. Figure 2a, b**), indicating that TSPO specifically mediates the recruitment of NLRP3 to mitochondria.

To further visualise NLRP3 translocation during inflammation activation, a proximity ligation assay (PLA) was performed to detect spatial proximity between NLRP3 and the mitochondrial marker SDHA (Fig. 2**e,**

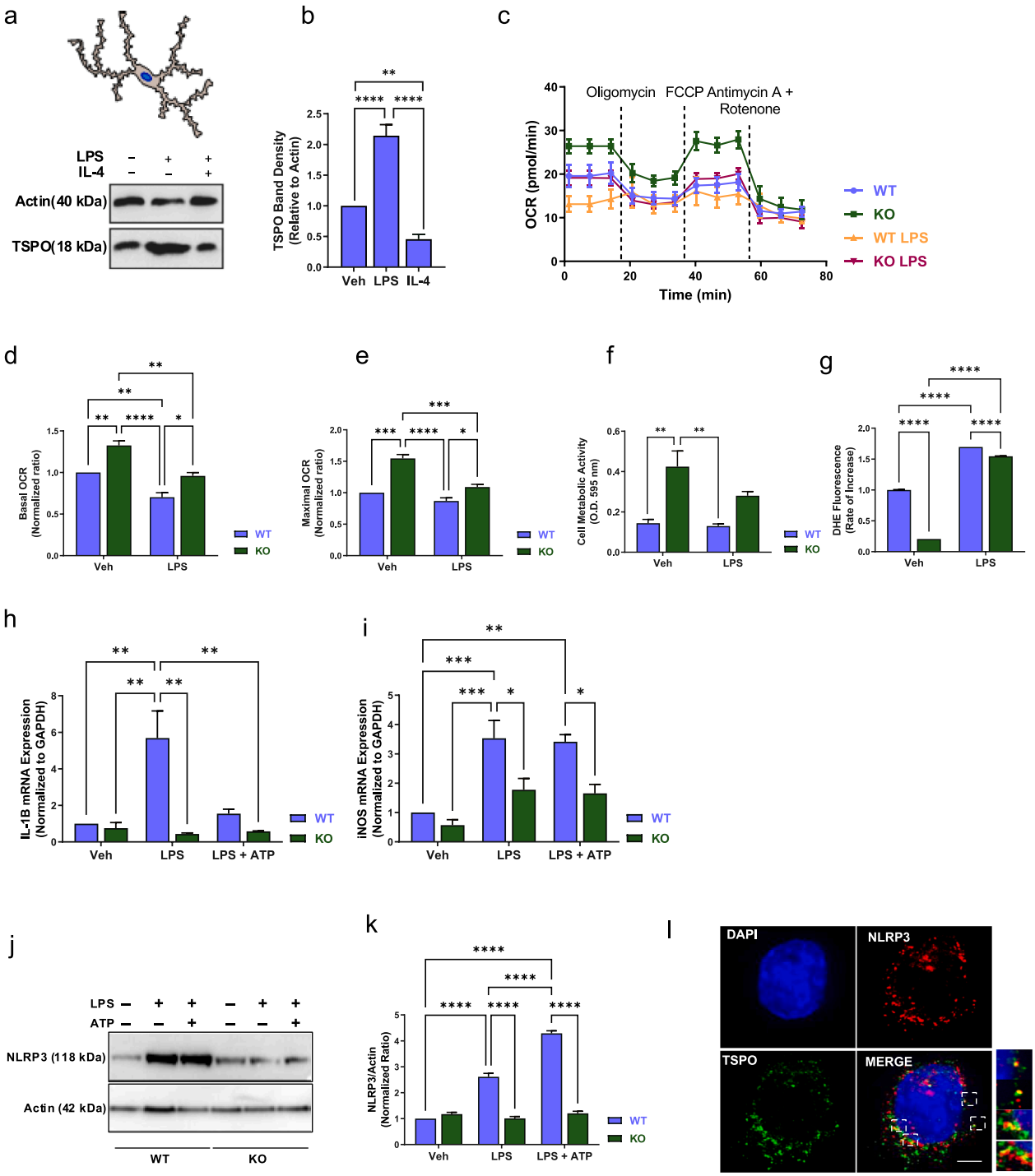

Fig. 1. Characterization of TSPO-knockout microglial cells. a, b) The anti-inflammatory cytokine IL-4 does not promote TSPO expression. Western blotting analysis of TSPO protein levels in BV2 cells treated with LPS (100 ng/mL) or IL-4 (20 ng/mL) (a) and relative quantification (b). c,d,e) Bioenergetic profiles of WT and TSPO KO BV2 cells at rest and after 24 h LPS treatment (100 ng/mL). Extracellular flux analysis was carried out using a standard Mito Stress Test kit with 1.5 μM oligomycin, 1 μM FCCP, and 0.5 μM rotenone/antimycin A (c). OCR values, expressed as pmol O_2/min, were used to calculate basal respiration (difference between OCR at rest and after rotenone/antimycin A administration) (d) and maximal respiratory capacity (difference between OCR under FCCP treatment and following the addition of rotenone/antimycin A) (e). The analysis indicates that TSPO KO cells have a higher metabolic capacity than WT. f) MTT viability assay showing increased mitochondrial activity in TSPO KO cells (OD three times higher than WT), which is retained even after treatment with LPS (100 ng/mL, 24 h). g) Analysis of intracellular ROS levels in WT and TSPO KO cells using the red fluorescent superoxide indicator DHE. Cells were incubated with either vehicle (Veh) or LPS (100 ng/mL, 24 h). TSPO KO BV2 cells have significantly lower levels of ROS when compared to WT cells, either treated or untreated. h,i) qPCR analysis of inflammatory marker expression. Expression levels of the proinflammatory cytokine IL-1β B (h), and inducible nitric oxide synthase (iNOS) (i) in WT and TSPO KO BV2 cells treated with either vehicle control, LPS (100 ng/mL, 24 h) or LPS followed by ATP (2.5 mM, 30 min). Data are reported as fold change in gene expression over control WT cells j, k) Western blotting analysis of NLRP3 protein levels in WT and TSPO KO BV2 cells at rest and after FCCP, LPS or LPS/ATP treatments (as described above). The representative blot (j) indicates that both LPS and LPS/ATP-induced activation result in a significant upregulation in NLRP3 protein expression in WT cells only, while NLRP3 levels don't change when TSPO is ablated, as quantified (k). l) Immunocytochemistry analysis showing the co-localisation of TSPO (green) and NLRP3 (red) in BV2 cells. Nuclei were counterstained with DAPI (blue).

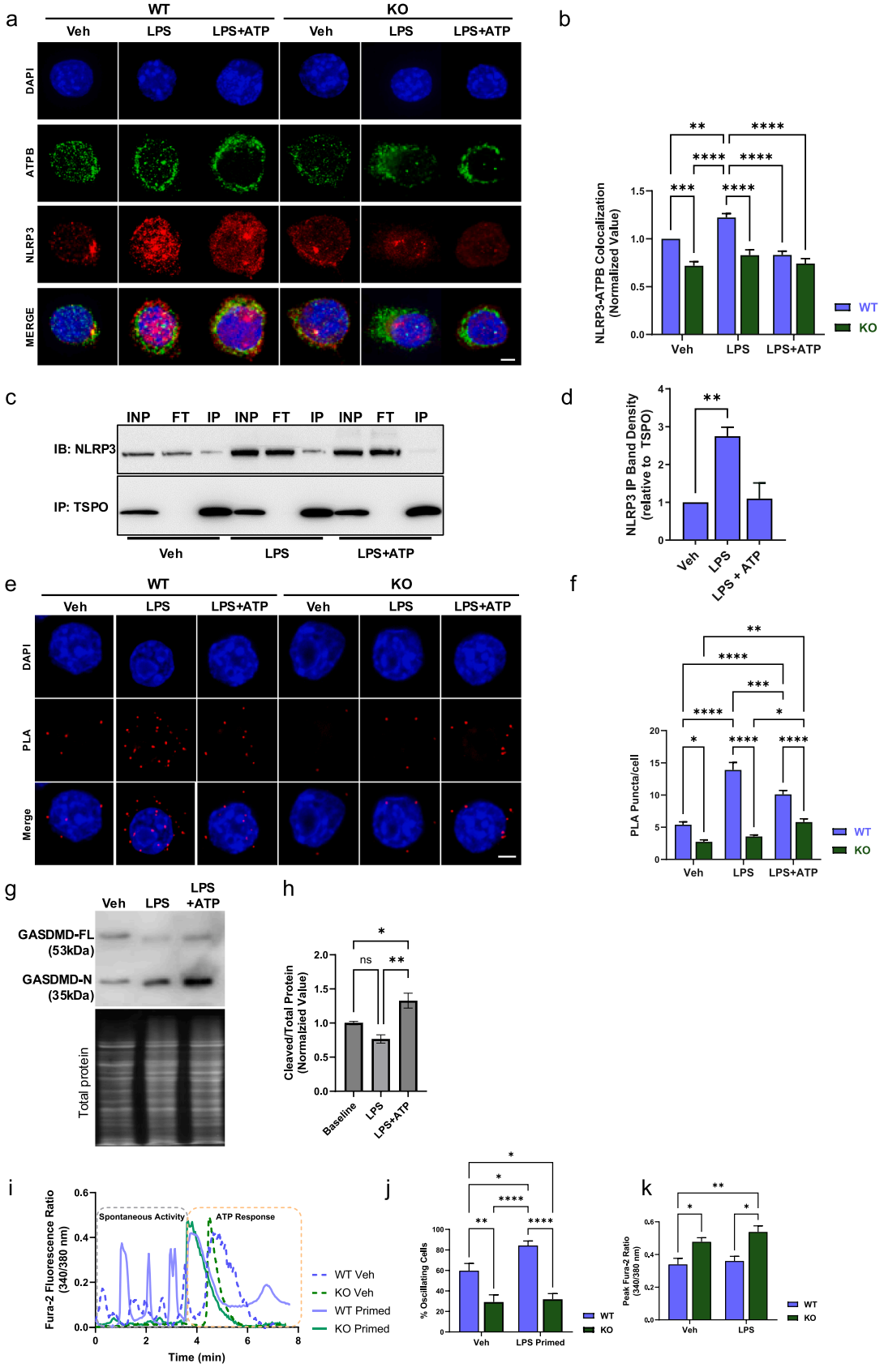

(caption on next page)

Fig. 2. TSPO ablation prevents NRLP3 stabilisation on mitochondria and represses Ca^{2+} accumulation in the cytosol. a, b) Immunocytochemistry analysis of occupancy of mitochondria by NLRP3 in LPS- and LPS/ATP-activated WT and TSPO KO BV2 cells (as previously described). The representative images (a) show BV2 cells stained with anti-NLRP3 (red) and anti-ATP synthase subunit beta (ATPB) (green) antibodies. The quantification of the co-localisation between the two fluorescent signals is reported in panel b. Knocking out TSPO inhibits pro-inflammatory mitochondrial recruitment of NLRP3. c, d) Co-Immunoprecipitation between TSPO and NRLP3 in LPS- and LPS/ATP-activated BV2 cells (n = 4). Panel d highlights the quantification of the interaction between the two proteins under LPS treatment. e, f) Proximity Ligation Assay (PLA) between Succinate dehydrogenase A (SHDA) and NLRP3 in BV2 WT and TSPO KO cells, untreated, primed with LPS (100 ng/mL LPS, 24 h) or activated with LPS followed by ATP (2.5 mM, 30 min). Relative quantifications in panel f g, h) Representative western blot analysis of full-length and cleaved GASDMD in WT cells following LPS or LPS+ATP treatment (g). Relative quantification of cleaved GASDMD is shown in panel h. i) Live-cell imaging analysis of intracellular Ca^{2+} dynamics in resting and primed (100 ng/mL LPS, 24 h) BV2 cell lines. Intracellular Ca^{2+} levels were monitored by using the ratio metric fluorescent Ca^{2+} indicator Fura-2 AM, before and after the addition of ATP (100 μM). Representative traces of the Fura-2 ratio at rest (spontaneous activity) and after ATP administration are specifically reported in untreated and LPS-treated cells. j) Quantification of the intracellular Ca^{2+} peak response in the conditions described above. k) Quantification of the percentage of oscillating cells in BV2 WT and TSPO KO cell lines in resting conditions or activated by LPS after the addition of ATP.

f). Consequently, NLRP3 translocation induced the cleavage of GASDMD following ATP stimulation, indicating the full activation of the NLRP3 signalling [31] (Fig. 2**g, h**).

WT BV2 cells exhibited more abundant PLA puncta compared to KO BV2 cells across all treatment conditions. LPS treatment induced a pronounced increase in the number of puncta, which moderately decreased after ATP stimulation. In contrast, LPS failed to promote NLRP3 accumulation at mitochondria in KO cells. Collectively, these results demonstrate that TSPO modulates inflammatory signalling by mediating the mitochondrial recruitment of NLRP3 during the priming stage, which is a critical step in inflammasome assembly [32].

In addition to changes in NLRP3 subcellular localization, inflammasome assembly is also regulated by intracellular Ca^{2+} dynamics [3,33,34]. Previous studies have demonstrated a critical role for calcium mobilisation in NLRP3 inflammasome activation [35]. Dolmetsch *et al.* showed that the expression of pro-inflammatory transcription factors was regulated by Ca^{2+} oscillation [36]. More recently, it is reported that Ca^{2+} oscillations can be transduced into downstream signalling cascades that drive the transcription of pro-inflammatory genes such as *TNF* and *IL8*[37]. Consistent with this, our live-cell results recording revealed that cytosolic Ca^{2+} oscillation is an intrinsic feature of WT BV2 cells, which is significantly intensified following LPS treatment (Fig. 2**i-k**), indicating WT BV2 cells are primed for inflammatory activation. In contrast, KO cells exhibited only weak Ca^{2+} oscillations, which remained low even after LPS treatment. This suggests that in the absence of TSPO, inflammatory signalling remains in an inactive state despite the presence of inflammatory cues.

3.3. TSPO deletion enhances mitophagy during pro-inflammatory activation in BV2 cells

To obtain a global overview of transcriptional changes induced by TSPO depletion, we performed RNA-Seq analysis of WT and TSPO knockout (KO) BV2 cells under basal and LPS-stimulated conditions. The results revealed a distinct transcriptomic profile in KO cells, particularly involving genes related to the NLRP3 inflammasome and autophagy/mitophagy pathways (Fig. 3**a, Supp. Figure 3a**). Overall, TSPO knockout led to downregulation of NLRP3 inflammasome components and upregulation of autophagy- and mitophagy-related genes.

To validate these findings, we looked into the mitochondria network in WT and KO BV2 cells and examined autophagy and mitophagy markers. At the basal level, WT cells displayed a greater mitochondrial network compared to KO cells, as revealed by mitoTracker staining (Fig. 3**b**, **c**). Upon LPS stimulation, the LC3-II/LC3-I ratio was significantly increased in KO cells, whereas WT cells remained unchanged (Fig. 3**d, e**), indicating enhanced autophagic flux in KO BV2 cells. Both FCCP and LPS treatment induced p62 accumulation on mitochondria, but the extent was markedly stronger in KO cells (Fig. 3**f, g**), suggesting restrained mitophagy initiation in the presence of TSPO. Consistently, PARK2 (Parkin) levels were elevated basally and further increased upon LPS or FCCP treatment in KO cells compared to WT (Fig. 3**h, i**). Consequently, extensive mitochondrial ubiquitination was also detected in KO cells upon LPS and LPS+ATP treatment (**Supp. Figure 3b,c**). In response to LPS treatment, we checked the autophagy flux which proved unmodified by the absence or presence of TSPO despite modfications in the mitochondrial content.

In parallel, MTCO1, a mitochondrial inner membrane protein, remained stable in WT cells but was significantly reduced in KO cells following LPS or LPS+ATP treatment (Fig. 3**j, k**), reflecting enhanced mitophagic clearance of mitochondria in the absence of TSPO. Collectively, these results demonstrate that TSPO depletion enhances mitophagy and mitophagy-mediated mitochondrial clearance, while WT cells maintain mitochondrial integrity.

3.4. TSPO is required for the LPS-induced nuclear retro-translocation of NF-κB

The results described above indicate that TSPO indeed affects both the expression and subcellular localisation of NLRP3. Given previous reports showing that NF-κB is a major upstream regulator of NLRP3 [32], we hypothesised that TSPO deficiency may also impact NF-κB. We first observed that during LPS-induced inflammatory activation, TSPO expression correlated positively with NF-κB, particularly during the priming phase, where LPS treatment induced synchronous upregulation of both TSPO and NF-κB (Fig. 4**a–c**). TSPO deletion abolished the LPS-induced NF-κB upregulation, suggesting that LPS-induced NF-κB upregulation is TSPO-dependent.

We then examined NF-κB translocation during BV2 cell activation. ICC results showed that in resting cells, NF-κB remained cytoplasmic in both WT and KO cells. LPS treatment induced spontaneous perinuclear accumulation of mitochondria and NF-κB in WT cells, whereas in KO cells, NF-κB remained a cytoplasmic distribution (Fig. 4**d, e**). Subcellular fractionation further confirmed prominent nuclear translocation of NF-κB in WT cells, as evidenced by a significant shift of signal from the cytosolic to the nuclear fraction (Fig. 4**f–h**). This translocation was absent in KO cells unless they were challenged with combined LPS and ATP. Together, these results demonstrate that TSPO is necessary for the retro-translocation of NF-κB, a key event during the priming stage of inflammatory activation.

We next investigated the role of TSPO in neuroinflammation, specifically in microglia–neuron interactions, using a conditioned media (CM) assay. As illustrated in Fig. 4**i**, both WT and KO BV2 cells were treated with vehicle or LPS for 24 h, and the resulting microglial conditioned media (Mic-CM) were applied to N2a neuroblastoma cells for 24 h. LDH assays revealed that Mic-CM from LPS-treated WT BV2 cells induced more N2a cell death than Mic-CM from LPS-treated TSPO KO cells (Fig. 4**j. k**), indicating that TSPO loss reduces microglia-mediated neurotoxicity, likely through suppression of pro-inflammatory cytokine release. Additionally, KO cells showed reduced sensitivity to LPS-induced cell death (Fig. 4**k**), suggesting that TSPO ablation mitigates pro-inflammatory forms of cell death, such as pyroptosis.

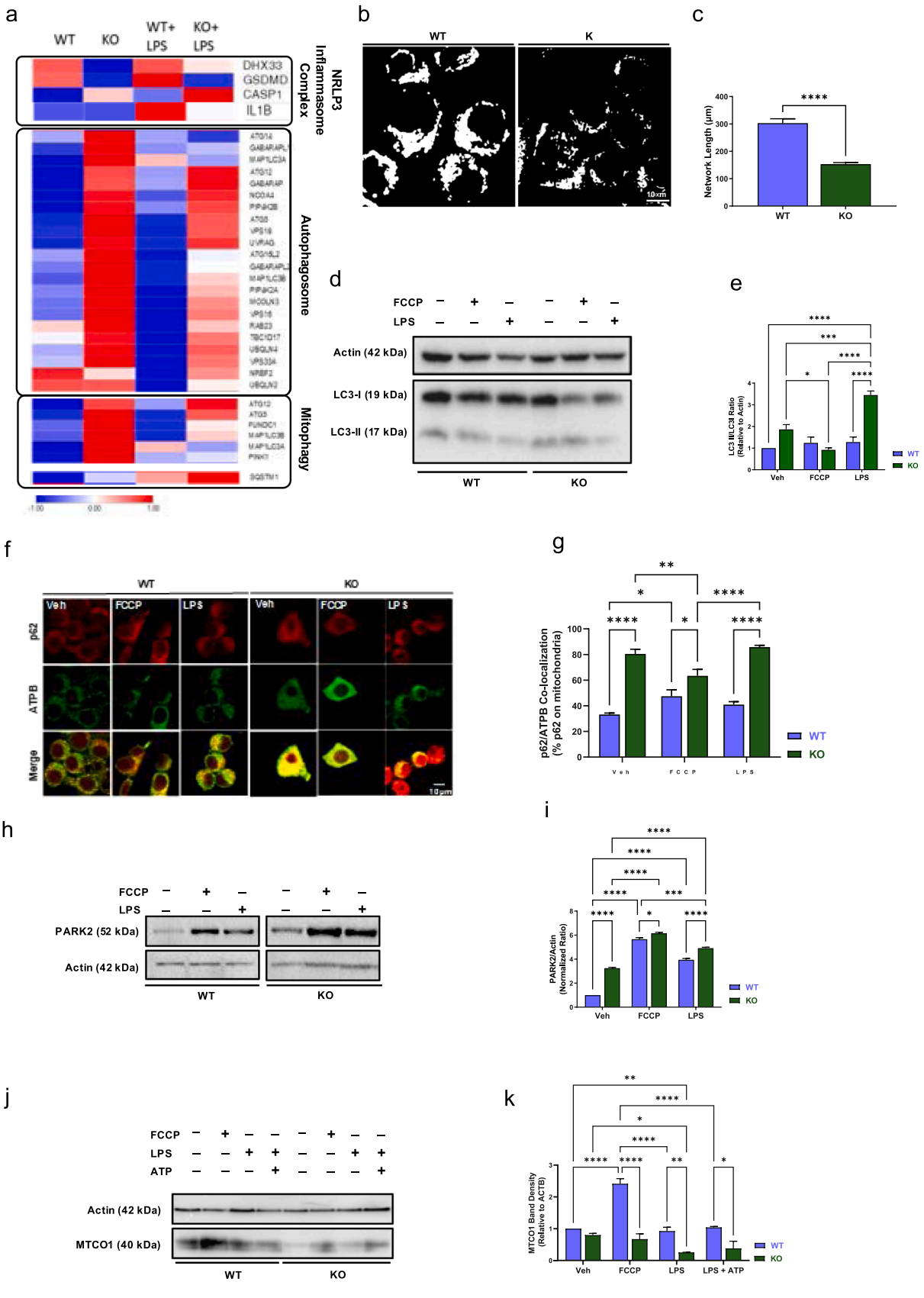

(caption on next page)

Fig. 3. TSPO represses macro and targeted autophagy during microglial cell activation. a) Heat maps of the RNA-seq profiles in BV2 WT and BV2 TSPO KO cells in resting condition and after LPS treatment (100 ng/mL, 24 h), highlighting the genes differently expressed related to NLRP3 inflammasome complex, autophagosome or mitophagy. b, c) Mito-tracker staining of mitochondrial network WT and TSPO KO BV2 cells (n = 3)(b). Relative quantification is shown in panel c d, e) Measurement of LC3 lipidation (LC3-II formation) in WT and TSPO KO BV2 cells following 24 h treatment with LPS (100 ng/mL, 24 h) or FCCP (10 μM, 24 h). Both LC3 bands (d) were quantified and the LC3-II: LC3-I ratio of expression was calculated (e) to compare LC3 lipidation (LC3-II formation) between samples before and after treatment. TSPO KO cells have a higher LC3-II: LC3-I ratio both at rest and following LPS-induced activation, suggesting that the autophagic flux increases in the absence of TSPO. f, g) Representative co-immunocytochemical analyses of SQSTM1/P62 and ATPB in BV2 WT and BV2 TSPO KO microglial cells, untreated, exposed to LPS or LPS+ATP (f). Panel g shows the histogram reporting the relative quantification. h, i) Representative immunoblot (h) and densitometry analysis (i) of mitochondrial Parkin levels in WT and TSPO KO BV2 cells at rest and following treatment with either FCCP (10 μM, 24 h) or LPS (100 ng/mL, 24 h). TSPO KO cells are characterised by increased basal expression of Parkin. j, k) Western blotting analysis of MTCO1 protein levels in WT and TSPO KO BV2 cells at rest and following treatment with either FCCP (10 μM, 24 h), LPS (100 ng/mL, 24 h) or LPS (100 ng/mL, 24 h)/ATP (2.5 mM, 30 min). As presented in panel j and quantified in panel k, TSPO KO cells have an overall decreased expression of MTCO1, the level of which does not change following treatments. MTCO1 expression is instead greatly induced by FCCP in WT cells.

3.5. TSPO as a pharmacological target for controlling inflammatory responses

Previous studies have highlighted TSPO as a potential in vivo biomarker of mitochondrial pathology for PET imaging. To further evaluate its potential as a pharmacological target for mitigating pathological neuroinflammation, we tested the effects of a recently developed, highly specific TSPO ligand,18F-GE-180 (S-N, N-diethyl-9-[2–18F-fluoroethyl]-5-methoxy-2,3,4,9-tetrahydro-1H-carbazole-4-carboxamide). GE-180, the lead compound from a new series of tricyclic indoles with high TSPO affinity, has been developed as a PET tracer for in vivo TSPO imaging [38,39] (Fig. 5**a–c**). GE180 displayed high specific binding affinity to TSPO with low noise nonspecific noise [38,39]. GE-180 has been used for detecting TSPO in mice and human brain [40,41]. GE-180 treatment didn't alter mitochondria morphology (Fig. 5**d, e**).In LPS-stimulated cells, GE-180 attenuated microglial activation in WT cells, as reflected by CD68 and nitrite ions level (Fig. 5f-h), as well as the rescue of mitochondria membrane potential (**Supp. Figure 4a, b**). In contrast, TSPO KO cells showed no response to GE-180, indicating that GE-180 specifically targets TSPO-mediated signalling. Consistently, GE-180 reduced LPS-induced NF-κB retro-translocation in WT cells (Fig. 5**i, j**). Together, these results demonstrate that TSPO is a critical mediator of microglial pro-inflammatory activation, which can be selectively inhibited by GE-180.Integrating our findings, we propose a model in which TSPO functions as a multi-level regulator of the microglial inflammatory cascade (Fig. 6**)**.

4. Discussion

Our study identifies TSPO as a mitochondrial regulator of murine microglial activation, via the recruitment of NLRP3 and the assembly of the inflammasome complex through NF-κB–dependent retro-translocation.

TSPO, which strongly upregulates in Iba-1 positive microglia of injured mouse brain (**S**Fig. 1**a,b**), is markedly enriched upon LPS stimulation in BV2 microglial cells, whereas it is suppressed by the anti-inflammatory cytokine IL-4 (**Fig. 1a,b**). These results resemble previous findings on TSPO upregulation as a distinctive feature of activated glial cells across both neurodegenerative and neurotraumatic conditions [42], but a novel underlying regulatory mechanism is proposed.

Here, we demonstrate thatTSPO-deficient BV2 cells show an increased basal mitochondrial respiration, which isn't remodelled in response to the LPS-induced metabolic shift, as recorded in the wild-type counterpart (Fig. 1**c-f**). The bioenergetic profile, dictated by the loss of TSPO, was also associated with lower cytosolic ROS levels and reduced expression of pro-inflammatory markers such as IL-1β, iNOS, and NLRP3 (Fig. 1**g-k**) [43,44]; indicative of a metabolic rewiring necessary for microglial activation [45–48]. Additionally, our imaging analyses revealed TSPO as a binding partner of NLRP3 (Fig. 1**l**), suggesting a mechanistic link. Inflammasome activation is a two-step process involving priming (**I**), during which NLRP3 and pro-IL-1β are transcriptionally upregulated by NF-κB, and activation (**II**), during which NLRP3 assembles into multimolecular complexes at mitochondria and at the mitochondrial sites of contact with the associated organelles in response to secondary danger signals such as ATP [49]. Our data reveal that TSPO is required for the first of these two steps: the mitochondrial recruitment of NLRP3. In WT BV2 cells, LPS treatment induced colocalization of NLRP3 and mitochondria thus promoting the subsequent inflammasome clustering upon ATP stimulation (Fig. 2**a,b**). Consistent with the ICC results, the co-immunoprecipitation assays showed that TSPO physically associates with NLRP3 under inflammatory conditions (Fig. 2**c,d**). Such interaction peaks during the LPS-priming phase but is released further upon ATP stimulation, supporting the role of TSPO as the transient mitochondrial docking site that facilitates the spatial organisation of inflammasome components [50,51]. This function may parallel the role of other mitochondrial adaptors, such as MAVS and TOM70, which regulate immune signalling through localised protein-protein interactions [52,53]. Notably, the localisation and clustering of ASC, another essential inflammasome adaptor, were not affected by TSPO deletion, underscoring the specificity of the TSPO–NLRP3 interplay (Fig. 2 **c-f**). The latter was sufficient to the activation of the downstream cascade, as it is well exemplified by Gasdermin cleavage (Fig. 2 **g,h).**

Inflammasome activation is known to be modulated by cytosolic Ca^{2+} flux and oscillations [36,37]. Live-cell Ca^{2+} imaging experiments revealed that WT BV2 cells display robust cytosolic Ca^{2+} oscillations, which become even higher upon LPS stimulation, whereas TSPO-deficient cells do not exhibit a similar pattern (Fig. 2 **i-k**). Given that TSPO has been implicated in the regulation of mitochondrial Ca^{2+} uptake through its interaction with the voltage-dependent anion channel (VDAC) and TOM40 [54,55], the lack of cytosolic Ca^{2+} oscillations in KO cells indicates that the mitochondrial compartment in these cells handles the cation better than the WT nterpart. TSPO acts therefore as a rheostat of Ca^{2+}-dependent signaling cascades [56], contributing to the activation and tonicity of inflammasome signalling [57].

In keeping with this, RNA-seq revealed that repression of TSPO expression leads to transcriptional upregulation of autophagy and mitophagy pathways at both the basal level and under LPS treatment (Fig. 3 **a**). Correspondingly, WT cells displayed a greater mitochondrial network compared to KO cells (Fig. 3 **b,c**) thereby implying that through regulating mitophagy, TSPO maintained a bigger platform for the rapid execution of the inflammatory signalling via the mitochondria [48,54, 58,59]. Substantiating this notion, depletion of TSPO resulted in higher mitophagy, evidenced by enhanced LC3 lipidation, elevated mitochondrial recruitment of p62 (Fig. 3 **d-g)**. This phenotype was further supported by increased PARK2 expression, ubiquitination and reduced level of mtDNA encoded protein MTCO1 (Fig. 3 **h-k).** A key reduction of mitochondrial content, triggered by both FCCP and LPS, which is independent of autophagy flux (**SFig. 3 b-f**).

Mitophagy serves as a quality control mechanism that eliminates damaged mitochondria to prevent excessive ROS and inflammation [54, 56]. However, excessive mitophagy can also deplete the mitochondrial pool necessary for innate immune signalling [60,61]. Our findings suggest that by maintaining mitochondrial activity at an optimal level

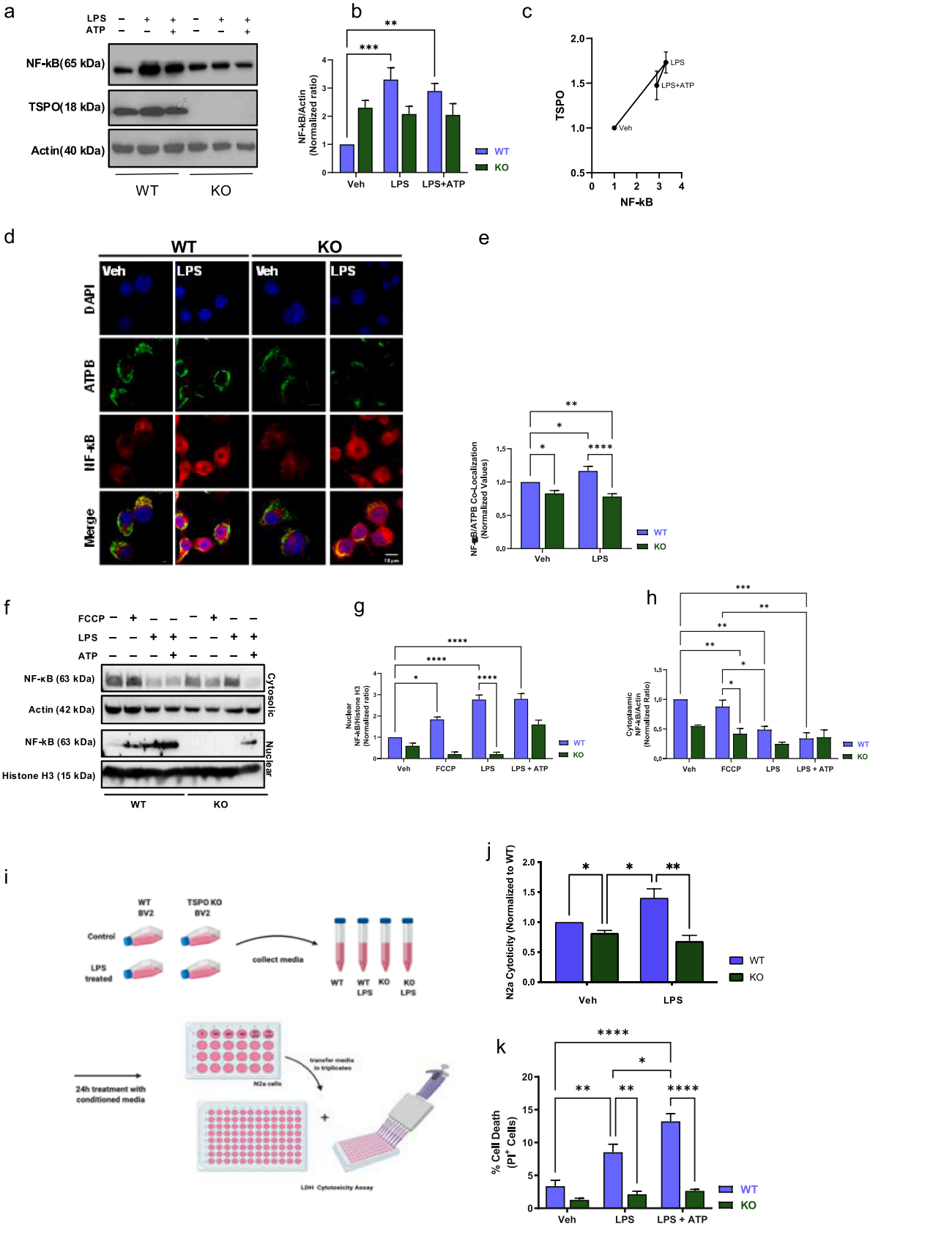

(caption on next page)

Fig. 4. TSPO engages NF-kB in microglial pathogenic signalling. a, b, c) Western blotting analysis of NF-kB and TSPO protein levels in WT and TSPO KO BV2 cells at rest and following treatment with either LPS (100 ng/mL, 24 h) or LPS (100 ng/mL, 24 h)/ATP (2.5 mM, 30 min). As presented in panel a and quantified in panel b, LPS treatment induces an increase in the expression levels of NF-kB. Moreover, panel c illustrates the correlation between the expression levels of TSPO and NF-kB proteins. d, e) Fluorescence ICC analysis of LPS-induced NF-κB nuclear translocation in WT and TSPO KO BV2. Cells were treated with 100 ng/mL LPS for 24 h. Representative images (d) showing NF-κB immunostaining (red) in combination with DAPI nuclear counterstain (blue). The levels of NF-κB nuclear fluorescence, reported in panel e, indicate that TSPO ablation inhibits LPS-mediated nuclear translocation of NF-κB. f, g, h) Analysis of NF-κB cytosolic and nuclear translocation in WT and TSPO KO BV2 cells following pro-inflammatory stimuli. Cells were treated with either FCCP (10 μM, 4 h), LPS (100 ng/mL, 24 h) or LPS/ATP (100 ng/mL LPS for 24 h followed by 2.5 mM ATP for 30 min). Cytosolic and nuclear fractions were then used to monitor the relocation of NF-κB between the two compartments via Western blotting. The representative blots (f) and respective densitometry analyses (g, h) show that treatment with LPS or LPS/ATP causes a significant translocation of NF-κB into the nucleus in WT cells, which is hampered by the lack of TSPO. i, j) Analysis of microglia-induced neurotoxicity in mouse N2a cells exposed for 24 h to Mic-CM media from either untreated or LPS-treated (100 ng/mL, 24 h) WT and TSPO KO BV2 cells. WT BV2 cell Mic-CM media induced neuronal cytotoxicity, which was measured through quantification (j) of LDH released in the extracellular environment. N2a cells treated with TSPO KO cell Mic-CM did not show signs of cytotoxicity. k) Quantification of changes in cell death as measured by PI inclusion between WT and KO BV2 cells treated with LPS (24 h using 100 ng/mL) or LPS ATP (24 h using 100 ng/mL followed by 30 min using 2.5 mM ATP) to induce pyroptosis. TSPO KO protects from LPS-induced pyroptosis.

for signalling rather than degradation, TSPO sustains inflammatory activation.

Nuclear translocation of NF-κB represents a central event in the priming phase of inflammatory activation [62] In recent years, accumulating evidence has indicated that mitochondrial retrograde signalling functions as the underlying orchestrator of NF-κB nuclear translocation during microglial activation [24,63]. Our data show that TSPO is required for NF-κB upregulation and nuclear translocation in microglia during the LPS-induced priming phase (Fig. 4 **a-h**). Upon LPS stimulation, WT BV2 cells exhibited pronounced perinuclear accumulation of mitochondria, which was concomitant with marked NF-κB nuclear translocation. On the other hand, TSPO-deficient cells failed to show such a redistribution, providing evidence for a coordinated spatiotemporal interplay between mitochondria and the nucleus likely to occur at the domains of contacts between these two organelles. TSPO content is suggested to be essential for microglial upscaling of the inflammasome pathway.

The functional relevance of TSPO-dependent microglial activation was further validated using a conditioned media assay to predict *in vivo* toxicity. Media from LPS-treated WT microglia caused substantial neuronal death in N2a cells, whereas media from LPS-treated TSPO-KO cells elicited minimal neurotoxicity (Fig. 4 **i-k**). This indicates that TSPO-dependent inflammatory activation in microglia directly contributes to neuronal injury, likely through cytokine and nitric oxide release. Moreover, TSPO deletion conferred protection against LPS-induced microglial cell death, suggesting that it may also modulate pyroptotic pathways [64]. These findings underscore the dual role of TSPO in both amplifying inflammatory signaling and sensitising microglia to inflammatory stress [65].

While acute neuroinflammatory responses can be protective, chronic or excessive neuroinflammation contributes to neurotoxicity [66,67]. Given the importance of TSPO in promoting pro-inflammatory activation, fine-tuning TSPO activity is particularly critical for maintaining the homeostasis and functional integrity of the nervous system [68,69].

The pharmacological inhibition experiments with GE-180 further consolidate TSPO's role as a druggable target. GE-180, a high-affinity TSPO ligand originally developed as a PET imaging tracer (Fig. 5 **a,b**), effectively reduced microglial activation, nitric oxide release, and NF-κB nuclear translocation in WT but not in TSPO-deficient cells, confirming both effectiveness and specificity of action (Fig. 5 **d-h**). Meanwhile, in the current study, we demonstrate that depletion of TSPO leads to a divergent pattern of cytosolic Ca^{2+} handling in BV2 KO cells compared to WT cells. This finding extends our previous observations regarding the role of TSPO in coordinating mitochondrial and cytosolic Ca^{2+} homeostasis [56,70,71]. Moreover, our data suggest an additional mechanism by which TSPO ligands may modulate neuroinflammation by modifying Ca^{2+} signalling critical for the NLRP3 cascade activation [50].

In recent years, a growing body of evidence has demonstrated that, in the human brain, microglia-mediated immunomodulation is not necessarily associated with increased TSPO expression [72–75]. This discrepancy, on one hand, raised fundamental questions regarding the continued use of TSPO as a surrogate marker of human neuroinflammation, on the other, these findings prompted a re-evaluation of the TSPO role during immune cell activation.

In the present study, by using a TSPO-deficient immunogenic mouse model, we demonstrate that TSPO functions as a mitochondrial mediator during immune activation, contributing predominantly to the priming phase. In this sense, TSPO potentially modulates immune responsiveness through orchestrating mitonuclear communication and signalling competence, rather than through activation-induced upregulation. Hence, we propose a putative mechanistic framework to explain why TSPO, despite being an active participant in immune activation, its expression level does not closely correlate with the overall activation state.

TSPO ligands can therefore allow for functional modulation minimising confounding effects associated with variable protein expression. This will also corroborate further the substantial promise TSPO holds as a pharmacological target [76].

However, our findings must be interpreted in the context of species-specific differences between murine and human microglia. Indeed, murine and human microglia exhibit divergent activation kinetics, metabolic demands, and gene expression programs [77,78]. Therefore, to rigorously assess the necessity of TSPO in human immune cell activation, besides generating TSPO-deficient models, integrated studies combining both murine and human systems will be critical. They will allow the dissection of the stage-specific roles of TSPO and identification of TSPO-associated downstream partners and co-regulators.

In summary, our study identifies TSPO as a central mitochondrial regulator that integrates metabolic, structural, and transcriptional pathways to control microglial activation and neuroinflammatory outcomes. By linking mitochondrial function with inflammasome assembly and retro-translocation of NF-κB, TSPO strengthened the role of mitochondria as the hub that ensures a coordinated inflammatory response. Future investigations should focus on resolving the molecular interfaces between TSPO, NLRP3, and associated mitochondrial proteins, as well as determining whether TSPO-dependent signalling is conserved in other CNS-resident immune cells. Finally, it will be important to assess the long-term effects of TSPO ligands for interventional strategies in neurological diseases.

Authors Contribution

M.C. conceived, designed, and coordinated the project together with A.S. who has performed almost the entirety of the in-cell experiments, their analyses and curation including the data points attained with GE-180. T.G. performed ICC and PLA experiment. M. J. L.T. and Z. F. H. A. have run the work on animal tissues. M.R. conducted the biochemical assessment of mitochondrial ubiquitination, assisted A.S. in the autophagy/mitophagy experiments and conducted the co-immunoprecipitation analysis, its analysis and presentation. The data on intracellular Ca^{2+} signalling which were conceived by M.C., D.F, A.S. were conducted by D.F. and M.G.C. who assisted with their design too.

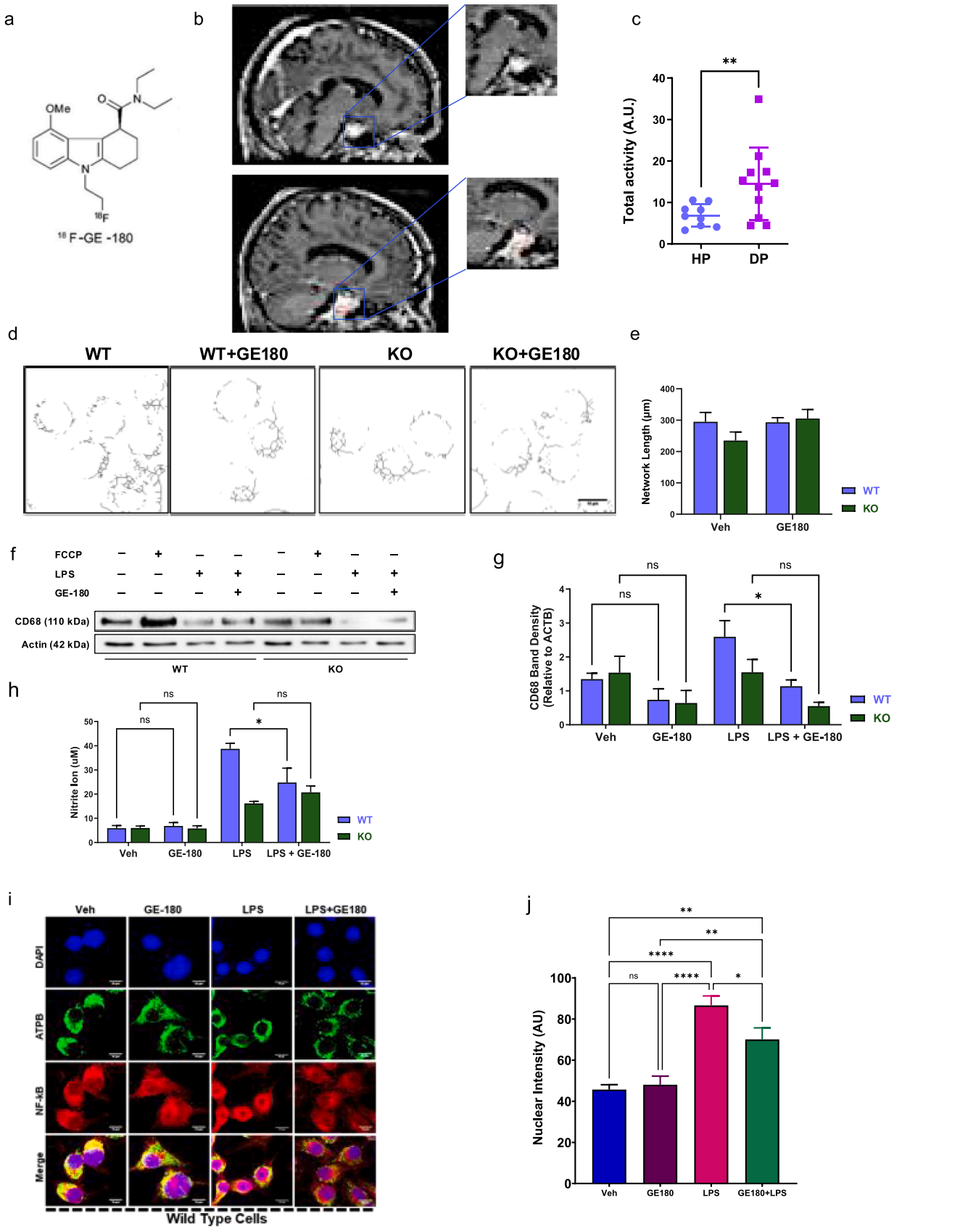

(caption on next page)

Fig. 5. TSPO is a pharmacological target to prevent pro-inflammatory microglial cell activation and associated demise. a, b, c) Molecular structure and improved standard uptake values (SUV) of the binding of TSPO ligand, GE-180. The figure shows the chemical structure of the compound (a) and representative PET-magnetic resonance imaging (MRI) scans with and without PMOD-generated "masks" on the carotid (b). Panel c contains quantifications demonstrating significant upregulation in the binding of ligand in the diseased patient (DP) over the healthy patient (HP). [18 F]GE-180 activity was evaluated around the maximal TSPO increase. Total disease activity measured for both groups of patients (HP: healthy patients; DP: diseased patients), normalised to standard uptake value (SUV) measured in carotid arteries (highlighted in multicolour rectangles at the bottom). d, e) Representative skeletonised images of mitochondrial morphology read via green mitotracker in BV2 cells treated with GE-180 and relative analysis (e). f, g) Immunoblotting analysis of CD68, Actin B and TSPO levels expression in WT and TSPO KO BV2 cells treated with LPS (100 ng/mL, 24 h), or GE-180 (100 nM, 24 h) with quantification in (g) that demonstrates a significant downregulation in CD68 accumulation in KO cells after LPS treatment. h) Griess reagent assay displays the changes in nitrite levels between WT and TSPO KO cells treated with LPS (100 ng/mL, 24 h), or GE-180 (100 nM, 24 h). The panel reiterates the reduction in the profile of neuroinflammatory markers in KO cells even after LPS administration. i, j) Immunocytochemical data on NF-kB retro-translocation on the nucleus in response to LPS (100 ng/mL, 24 h) alone or combined with GE-180 (100 nM, 24 h) in WT and TSPO KO cells. Nuclear intensity measured via co-localisation is reported in j.

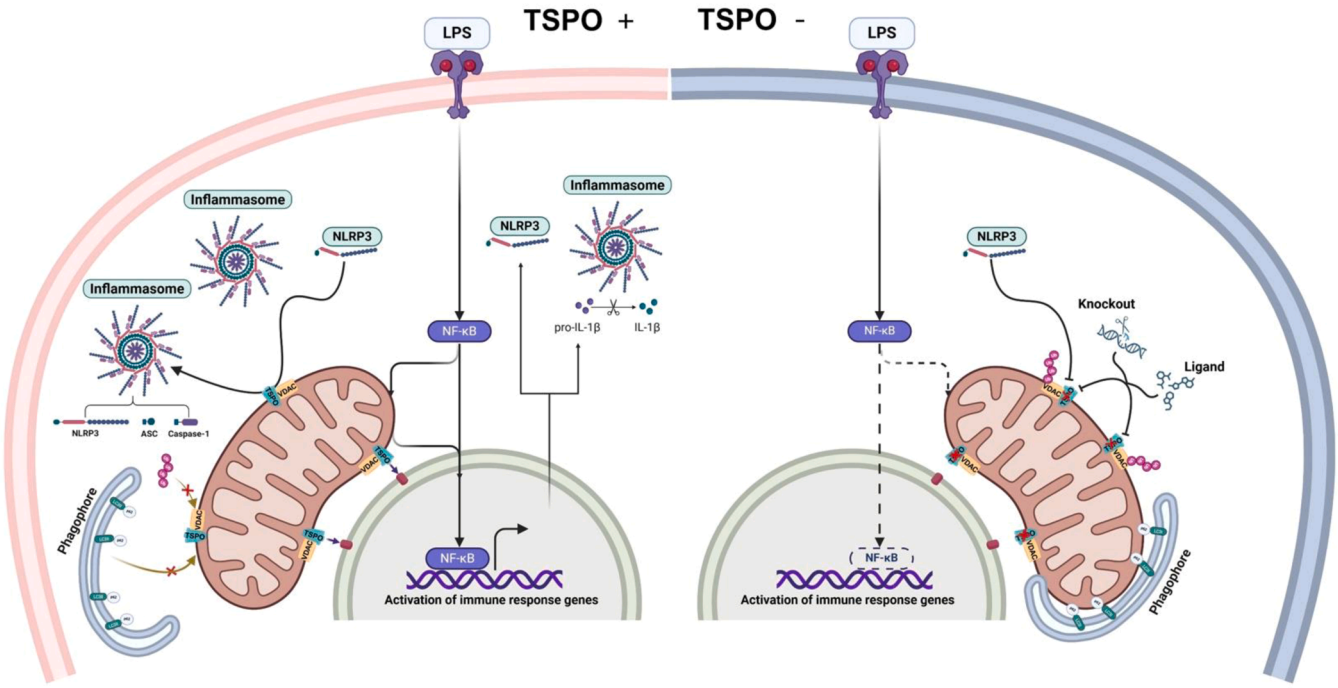

Fig. 6. NLRP3 inflammasome assembly and activation according to TSPO expression. Upon pro-inflammatory stimulation (e.g., LPS), TSPO is upregulated and facilitates mitochondrial recruitment of NLRP3 and retrograde translocation of NF-kB, driving transcriptional priming of pro-inflammatory genes. Concurrently, TSPO suppresses excessive mitochondrial integrity required for inflammasome assembly. In the absence of TSPO, this integrated network collapses, leading to enhanced mitophagy, defective inflammasome assembly and attenuated NF-κB translocation, collectively making microglia incapable of mounting a full pro-inflammatory response. Lack of TSPO promotes autophagic clearance of mitochondria, thereby impeding mitochondrial recruitment of NLRP3 and inflammasome assembly. TSPO ligand suppresses TSPO, ensuring an optimal level of inflammatory activation of BV2 cells.

M.G.C. finalized the assay on N2a cytotoxicity designed together with M. C. G.L preformed western blot analysis.

R.A., P.G. and D.X. performed the RNA-seq and their analysis. A.S. wrote the manuscript which was edited by M.C. and finalized in the current format with the key assistance of T.G. and M.R. All authors have critically reviewed and approved the manuscript.

CRediT authorship contribution statement

Michelangelo Campanella: Writing – review & editing, Supervision, Project administration, Funding acquisition, Data curation, Conceptualisation. **Aarti Singh**: Writing – original draft, Investigation, Formal analysis, Data curation. **Manuel Rigon**: Writing – review & editing, Validation, Investigation, Formal analysis, Data curation. **Tong Guo:** Writing – review & editing, Validation, Methodology, Formal analysis, Data curation. **Rosella Abeti, Marta Gramaça Caldeira, Danilo Faccenda, Paola Giunti, Gopinath Lakshmanan**: Investigation, Validation, Methodology, Formal analysis. **Dong Xia**: Software, Methodology, Formal analysis. **Jordi Lopez-Tremoleda, Zahra Falah Hassan Al-Khateeb**: Validation, Methodology, Formal analysis, Data curation.

Statement on animal experimentation

All animal procedures were carried out under an approved Project Licences (PE40BCDCE) by the Animal Welfare and Ethical Review Body at Queen Mary University of London and the UK Animals (Scientific Procedures) Act 1986. Methods for animal care and welfare, experimental procedures along with experimental planning including data randomization and blinding during data acquisition and analysis are reported in accordance with the ARRIVE 2.0 guidelines. In accordance with the WMA statement on animal use in biomedical research, the use of animals in this study were justified in the QMUL Ethical Committee.

Declaration of Competing Interest

This research was conducted in the absence of any commercial or financial relationships. However, Dr Singh and Prof. Campanella are named inventors of patent applications on the molecular and pharmacological regulation of COVID-19-mediated pyroptosis.

Acknowledgements

The research activities led by M.C. are supported by the following funders, who are gratefully acknowledged: Biotechnology and Biological Sciences Research Council [grant numbers BB/M010384/1 and BB/N007042/1; The European Research Council COG 2018–819600_FIRM; Fondation ARC pour la Recherche sur le Cancer ARCLEADER2022020004901; AIRC-MFAG 21903, Rotary Foundation and the GiME Charity. An iCase Studentship awarded by the BBSRC and co-funded by General Electric Healthcare has supported A.S. in her endeavours. We would like to thank Dr Andrew Hibbert for the help with the imaging data, Dr Ruby Chan for the assistance in the statistical analysis. GE-180 was a gift from GE Healthcare

Appendix A. Supporting information

Supplementary data associated with this article can be found in the online version at doi:10.1016/j.phrs.2026.108145.

References

[1] S.S. Ousman, P. Kubes, Immune surveillance in the central nervous system, Nat. Neurosci. 15 (8) (2012) 1096–1101.
[2] J.A. Smith, et al., Role of pro-inflammatory cytokines released from microglia in neurodegenerative diseases, Brain Res Bull. 87 (1) (2012) 10–20.
[3] D.S. Wang, et al., Anxiolytic-like effects of translocator protein (TSPO) ligand ZBD-2 in an animal model of chronic pain, Mol. Pain. 11 (2015) 16.
[4] J.D. Cherry, J.A. Olschowka, M.K.O. Banion, Neuroinflammation and M2 microglia: the good, the bad, and the inflamed, J. Neuroinflamm. 11 (2014) 98.
[5] P. Gurung, J.R. Lukens, T.D. Kanneganti, Mitochondria: diversity in the regulation of the NLRP3 inflammasome, Trends Mol. Med 21 (3) (2015) 193–201.
[6] R. Zhou, et al., A role for mitochondria in NLRP3 inflammasome activation, Nature 469 (7329) (2011) 221–225.
[7] L.M. Booshehri, H.M. Hoffman, CAPS and NLRP3, J. Clin. Immunol. 39 (3) (2019) 277–286.
[8] Z. Zhong, et al., New mitochondrial DNA synthesis enables NLRP3 inflammasome activation, Nature 560 (7717) (2018) 198–203.
[9] M.J. Kim, et al., SESN2/sestrin2 suppresses sepsis by inducing mitophagy and inhibiting NLRP3 activation in macrophages, Autophagy 12 (8) (2016) 1272–1291.
[10] F. Bonsack, S. Sukumari-Ramesh, TSPO: An Evolutionarily Conserved Protein with Elusive Functions, Int J. Mol. Sci. 19 (6) (2018).
[11] E.B. Souza, et al., Peripheral-type benzodiazepine receptors in endocrine organs: autoradiographic localization in rat pituitary, adrenal, and testis, Endocrinology 116 (2) (1985) 567–573.
[12] M.B. Rone, J. Fan, V. Papadopoulos, Cholesterol transport in steroid biosynthesis: role of protein-protein interactions and implications in disease states, Biochim Biophys. Acta 1791 (7) (2009) 646–658.
[13] D. Ory, et al., PET radioligands for in vivo visualization of neuroinflammation, Curr. Pharm. Des. 20 (37) (2014) 5897–5913.
[14] R. Rupprecht, et al., Translocator protein (18 kDa) (TSPO) as a therapeutic target for neurological and psychiatric disorders, Nat. Rev. Drug Discov. 9 (12) (2010) 971–988.
[15] K. Mages, et al., The agonistic TSPO ligand XBD173 attenuates the glial response thereby protecting inner retinal neurons in a murine model of retinal ischemia, J. Neuroinflamm. 16 (1) (2019) 43.
[16] R. Scholz, et al., Targeting translocator protein (18 kDa) (TSPO) dampens pro-inflammatory microglia reactivity in the retina and protects from degeneration, J. Neuroinflamm. 12 (2015) 201.
[17] J.B. Jia, et al., Novel TSPO-targeted Doxorubicin Prodrug for Colorectal Carcinoma Cells, Anticancer Res 40 (10) (2020) 5371–5378.
[18] M.C. Mendonça-Torres, S.S. Roberts, The translocator protein (TSPO) ligand PK11195 induces apoptosis and cell cycle arrest and sensitizes to chemotherapy treatment in pre- and post-relapse neuroblastoma cell lines, Cancer Biol. Ther. 14 (4) (2013) 319–326.
[19] N. Takai, et al., PK11195 enhances chemosensitivity to cisplatin and paclitaxel in human endometrial and ovarian cancer cells, Int J. Mol. Med 25 (1) (2010) 97–103.
[20] A.A. Crawshaw, N.P. Robertson, The role of TSPO PET in assessing neuroinflammation, J. Neurol. 264 (8) (2017) 1825–1827.
[21] L. Zhang, et al., Recent developments on PET radiotracers for TSPO and their applications in neuroimaging, Acta Pharm. Sin. B 11 (2) (2021) 373–393.
[22] Z. Zhong, et al., NF-κB Restricts Inflammasome Activation via Elimination of Damaged Mitochondria, Cell 164 (5) (2016) 896–910.
[23] J. Fan, V. Papadopoulos, Mitochondrial TSPO Deficiency Triggers Retrograde Signaling in MA-10 Mouse Tumor Leydig Cells, Int J. Mol. Sci. 22 (1) (2020).
[24] R. Desai, et al., Mitochondria form contact sites with the nucleus to couple prosurvival retrograde response, Sci. Adv. 6 (51) (2020).
[25] S.D. Wright, et al., CD14, a receptor for complexes of lipopolysaccharide (LPS) and LPS binding protein, Science 249 (4975) (1990) 1431–1433.
[26] P.J. Murray, Macrophage Polarization, Annu Rev. Physiol. 79 (2017) 541–566.
[27] D.R. Owen, et al., TSPO mutations in rats and a human polymorphism impair the rate of steroid synthesis, Biochem J. 474 (23) (2017) 3985–3999.
[28] X.J. Dai, et al., Activation of BV2 microglia by lipopolysaccharide triggers an inflammatory reaction in PC12 cell apoptosis through a toll-like receptor 4-dependent pathway, Cell Stress Chaperon.. 20 (2) (2015) 321–331.
[29] Y. Jia, et al., Ganoderic Acid A Attenuates LPS-Induced Neuroinflammation in BV2 Microglia by Activating Farnesoid X Receptor, Neurochem. Res 46 (7) (2021) 1725–1736.
[30] M.L. Pan, et al., Response Profiles of BV2 Microglia to IFN-γ and LPS Co-Stimulation and Priming, Biomedicines 11 (10) (2023).
[31] C. Wang, et al., NLRP3 inflammasome activation triggers gasdermin D-independent inflammation, Sci. Immunol. 6 (64) (2021) eabj3859.
[32] F.G. Bauernfeind, et al., Cutting edge: NF-kappaB activating pattern recognition and cytokine receptors license NLRP3 inflammasome activation by regulating NLRP3 expression, J. Immunol. 183 (2) (2009) 787–791.
[33] G. Eichhoff, B. Brawek, O. Garaschuk, Microglial calcium signal acts as a rapid sensor of single neuron damage in vivo, Biochim Biophys. Acta 1813 (5) (2011) 1014–1024.
[34] S. Koizumi, et al., UDP acting at P2Y6 receptors is a mediator of microglial phagocytosis, Nature 446 (7139) (2007) 1091–1095.
[35] T. Murakami, et al., Critical role for calcium mobilization in activation of the NLRP3 inflammasome, Proc. Natl. Acad. Sci. USA 109 (28) (2012) 11282–11287.
[36] R.E. Dolmetsch, K. Xu, R.S. Lewis, Calcium oscillations increase the efficiency and specificity of gene expression, Nature 392 (6679) (1998) 933–936.
[37] P. Nikpour, et al., Decoding calcium oscillation frequency in transcriptional regulation, bioRxiv (2025) 2025, 10.10.676024.
[38] H. Wadsworth, et al., 18F]GE-180: A novel fluorine-18 labelled PET tracer for imaging Translocator protein 18kDa (TSPO), Bioorg. Med. Chem. Lett. 22 (3) (2012) 1308–1313.
[39] H. Boutin, et al., 18F-GE-180: a novel TSPO radiotracer compared to 11C-R-PK11195 in a preclinical model of stroke, Eur. J. Nucl. Med Mol. Imaging 42 (3) (2015) 503–511.
[40] B. Liu, et al., In Vivo Detection of Age- and Disease-Related Increases in Neuroinflammation by 18F-GE180 TSPO MicroPET Imaging in Wild-Type and Alzheimer's Transgenic Mice, J. Neurosci. 35 (47) (2015) 15716–15730.
[41] P. Zanotti-Fregonara, et al., Head-to-Head Comparison of (11)C-PBR28 and (18)F-GE180 for Quantification of the Translocator Protein in the Human Brain, J. Nucl. Med 59 (8) (2018) 1260–1266.
[42] E.L. Werry, et al., Recent Developments in TSPO PET Imaging as A Biomarker of Neuroinflammation in Neurodegenerative Disorders, Int J. Mol. Sci. 20 (13) (2019).
[43] X. Dou, et al., Down-regulation of TSPO expression doesn't affect the productions of TNF-α, IL-1β and IL-6 in LPS-stimulated BV-2 microglia, Xi Bao Yu Fen. Zi Mian Yi Xue Za Zhi 30 (9) (2014) 897–900.
[44] P.N. Thai, et al., Cardiac-specific Conditional Knockout of the 18-kDa Mitochondrial Translocator Protein Protects from Pressure Overload Induced Heart Failure, Sci. Rep. 8 (1) (2018) 16213.
[45] K. Ceyzériat, et al., TSPO contributes to neuropathology and cognitive deficits in Alzheimer's disease, J. Neuroinflamm. 22 (1) (2025) 248.
[46] C. Betlazar, et al., The Translocator Protein (TSPO) in Mitochondrial Bioenergetics and Immune Processes, Cells 9 (2) (2020).
[47] Z. Gong, et al., Mitochondrial dysfunction induces NLRP3 inflammasome activation during cerebral ischemia/reperfusion injury, J. Neuroinflamm. 15 (1) (2018) 242.
[48] G. Scaini, et al., TSPO upregulation in bipolar disorder and concomitant downregulation of mitophagic proteins and NLRP3 inflammasome activation, Neuropsychopharmacology 44 (7) (2019) 1291–1299.
[49] K.V. Swanson, M. Deng, J.P.Y. Ting, The NLRP3 inflammasome: molecular activation and regulation to therapeutics, Nat. Rev. Immunol. 19 (8) (2019) 477–489.
[50] J.W. Lee, et al., A translocator protein 18 kDa ligand, Ro5-4864, inhibits ATP-induced NLRP3 inflammasome activation, Biochem Biophys. Res Commun. 474 (3) (2016) 587–593.
[51] G. Campbell, D.J. Mahad, Mitochondrial dysfunction and axon degeneration in progressive multiple sclerosis, FEBS Lett. 592 (7) (2018) 1113–1121.
[52] N. Subramanian, et al., The adaptor MAVS promotes NLRP3 mitochondrial localization and inflammasome activation, Cell 153 (2) (2013) 348–361.
[53] X.Y. Liu, et al., Tom70 mediates activation of interferon regulatory factor 3 on mitochondria, Cell Res 20 (9) (2010) 994–1011.
[54] J. Gatliff, et al., TSPO interacts with VDAC1 and triggers a ROS-mediated inhibition of mitochondrial quality control, Autophagy 10 (12) (2014) 2279–2296.
[55] D.-s Zhai, et al., TOM40 mediates the effect of TSPO on postpartum depression partially through regulating calcium homeostasis in microglia, J. Affect. Disord. 348 (2024) 283–296.
[56] J. Gatliff, et al., A role for TSPO in mitochondrial Ca(2+) homeostasis and redox stress signaling, Cell Death Dis. 8 (6) (2017) e2896.
[57] A. Lilienbaum, A. Israël, From Calcium to NF-κB Signaling Pathways in Neurons, Mol. Cell. Biol. 23 (8) (2003) 2680–2698.
[58] M. Frison, et al., The translocator protein (TSPO) is prodromal to mitophagy loss in neurotoxicity, Mol. Psychiatry 26 (7) (2021) 2721–2739.
[59] L. Issop, et al., Translocator Protein-Mediated Stabilization of Mitochondrial Architecture during Inflammation Stress in Colonic Cells, PLoS One 11 (4) (2016) e0152919.
[60] K. Chen, et al., Optineurin inhibits NLRP3 inflammasome activation by enhancing mitophagy of renal tubular cells in diabetic nephropathy, Faseb J. 33 (3) (2019) 4571–4585.

[61] N.P. Zhang, et al., Impaired mitophagy triggers NLRP3 inflammasome activation during the progression from nonalcoholic fatty liver to nonalcoholic steatohepatitis, Lab Invest 99 (6) (2019) 749–763.
[62] Q. Guo, et al., NF-κB in biology and targeted therapy: new insights and translational implications, Signal Transduct. Target. Ther. 9 (1) (2024) 53.
[63] Z. Wu, et al., LUBAC assembles a ubiquitin signaling platform at mitochondria for signal amplification and transport of NF-κB to the nucleus, Embo J. 41 (24) (2022) e112006.
[64] Y. Huang, W. Xu, R. Zhou, NLRP3 inflammasome activation and cell death, Cell Mol. Immunol. 18 (9) (2021) 2114–2127.
[65] F. Bonsack, C.H. Alleyne Jr., S. Sukumari-Ramesh, Resveratrol Attenuates Neurodegeneration and Improves Neurological Outcomes after Intracerebral Hemorrhage in Mice, Front Cell Neurosci. 11 (2017) 228.
[66] W. Zhang, et al., Role of neuroinflammation in neurodegeneration development, Signal Transduct. Target. Ther. 8 (1) (2023) 267.
[67] E.F. Fang, et al., Mitophagy inhibits amyloid-β and tau pathology and reverses cognitive deficits in models of Alzheimer's disease, Nat. Neurosci. 22 (3) (2019) 401–412.
[68] M. Azrad, et al., The TSPO Ligands 2-Cl-MGV-1, MGV-1, and PK11195 Differentially Suppress the Inflammatory Response of BV-2 Microglial Cell to LPS, Int J. Mol. Sci. 20 (3) (2019).
[69] K.R. Bae, et al., Translocator protein 18 kDa negatively regulates inflammation in microglia, J. Neuroimmune Pharm. 9 (3) (2014) 424–437.
[70] M. Campanella, G. Szabadkai, R. Rizzuto, Modulation of intracellular Ca2+ signalling in HeLa cells by the apoptotic cell death enhancer PK11195, Biochem Pharm. 76 (11) (2008) 1628–1636.
[71] C. Tamse, et al., The peripheral benzodiazepine receptor modulates Ca2+ transport through the VDAC in rat heart mitochondria, J. Clin. Basic Cardiol. 11 (1) (2008) 24–29.
[72] O.V. Chechneva, W. Deng, Mitochondrial translocator protein (TSPO), astrocytes and neuroinflammation, Neural Regen. Res 11 (7) (2016) 1056–1057.
[73] D.J. Daugherty, et al., The hGFAP-driven conditional TSPO knockout is protective in a mouse model of multiple sclerosis, Sci. Rep. 6 (1) (2016) 22556.
[74] M. Sadeghian, et al., Mitochondrial dysfunction is an important cause of neurological deficits in an inflammatory model of multiple sclerosis, Sci. Rep. 6 (2016) 33249.
[75] K. Zhou, et al., Recent Advances of the NLRP3 Inflammasome in Central Nervous System Disorders, J. Immunol. Res 2016 (2016) 9238290.
[76] E. Nutma, et al., Translocator protein is a marker of activated microglia in rodent models but not human neurodegenerative diseases, Nat. Commun. 14 (1) (2023) 5247.
[77] F.R. Sharp, G.C. Jickling, Modeling immunity and inflammation in stroke: differences between rodents and humans? Stroke 45 (9) (2014) e179–e180.
[78] B. Stansley, J. Post, K. Hensley, A comparative review of cell culture systems for the study of microglial biology in Alzheimer's disease, J. Neuroinflamm. 9 (1) (2012) 115.